Zeitschrift für Kristallographie 198, 177 – 212 (1992)
 – 0044-2968/92 $ 3.00 + 0.00

Crystal structures of the low-temperature quartz-type phases of SiO_2 and GeO_2 at elevated pressure

J. Glinnemann[1], H. E. King, Jr.[2], H. Schulz[3], Th. Hahn[1], S. J. La Placa[4] and F. Dacol[4]

[1] Institute of Crystallography, Rheinisch-Westfälische Technische Hochschule, Aachen, W-5100 Aachen, Federal Republic of Germany
[2] Exxon Research and Engineering Co., Annandale, NJ 0880, USA
[3] Institute of Crystallography and Mineralogy, University of München, W-8000 München 2, Federal Republic of Germany
[4] IBM T. J. Watson Research Center, Yorktown Heights, NY 10598, USA

Dedicated to Professor F. Liebau on the occasion of his 65th birthday

Received: July 23, 1988, revised January 2, 1991

Quartz / SiO_2 / GeO_2 / Pressure / Crystal chemistry / Crystal structures

Abstract. Lattice parameters and crystal structures of the low-temperature quartz-type ('low-quartz') forms (space group $P3_121$) of SiO_2 and GeO_2 were refined from single-crystal X-ray diffraction data under hydrostatic pressures up to 10.2 GPa for SiO_2 and 5.57 GPa for GeO_2. $R_w(F)$ values range from 2 to 5%.

Hexagonal unit-cell parameters for SiO_2: $a = 4.921(1)$, $c = 5.4163(8)$ Å at ambient conditions; $a = 4.604(1)$, $c = 5.207(1)$ Å at 10.2(1) GPa. For GeO_2: $a = 4.9844(2)$, $c = 5.6477(2)$ Å at normal pressure; $a = 4.750(1)$, $c = 5.548(5)$ Å at 5.57 GPa. Volume decrease, 16% for SiO_2 and 11% for GeO_2 is accomplished mainly by tetrahedral tilting, the rest arising from tetrahedral angle distortion.

GeO_2-quartz is an almost perfect high-pressure model for SiO_2-quartz: At 10 GPa the geometry of the SiO_2-quartz structure approaches that of GeO_2 at ambient pressure (e.g. similar values for c/a, atomic parameters, tetrahedral tilt angle, tetrahedral distortion). These values then further change for GeO_2 with increasing pressure reflecting increasing structural distortion.

The Si – O – Si angle decreases with pressure from 144.2(2) to 130.3(1)°, the Ge – O – Ge angle from 130.0(1) to 123.4(3)°. The Si...Si distance between vertex-connected tetrahedra shrinks from 3.0627(4) to 2.9152(8) Å,

the respective Ge...Ge distance from 3.1515(3) to 3.054(1) Å. Both distances, at maximum pressures, fall slightly below smallest reported values for silicates and germanates at ambient conditions. The variations in the angle T–O–T and the nonbonded distance T...T are nearly independent of changes in the T–O bond lengths.

The shortest O...O distance between unconnected tetrahedra decreases from 3.345(2) to 2.793(2) Å in SiO_2, and from 3.023(3) to 2.809(9) Å in GeO_2. For quartz this distance remains longer than the longest tetrahedral edge, which increases from 2.640(3) to 2.690(2) Å. For GeO_2 however, it shrinks to the second-shortest oxygen–oxygen distance in the structure; only two symmetry equivalent tetrahedral edges are shorter, 2.725(4) Å, at the maximum pressure. The two symmetry equivalent second-shortest intertetrahedral O...O distances in GeO_2 decrease from 3.192(2) to 2.926(6) Å, becoming shorter than the largest tetrahedral edge, which increases from 2.903(2) to 2.943(5) Å. Extrapolating these developments, the oxygen atoms would reach positions at the lattice points of a cubic body-centred lattice (Sowa, 1988).

Increasing tetrahedral distortion with pressure is displayed mainly by angle distortion. The quantity, DI(OTO) (Baur, 1974), increases from 0.6 to 2.6% for SiO_2 and from 2.5 to 4.2% for GeO_2. The longer Si–O bond remains constant at 1.614(2) Å, whereas the shorter one decreases from 1.605(2) to 1.599(2) Å. These values reflect the stiffness of the respective bonds. The changes in the Ge–O bond lengths are correspondingly small but are less regular with increasing pressure. The variations of bond angles O–T–O and respective tetrahedral edges are nearly independent of changes in the T–O bond lengths.

Tetrahedral distortion mechanisms are seen to differ in comparing changing pressure or temperature.

Introduction

Quartz has been the subject of numerous studies. Among the many reasons are: its importance as a mineral, its interesting physical properties, its commercial importance as a piezoelectric material and as a component of glass, and its comparatively simple crystal structure.

For SiO_2 the low-quartz form is the stable phase at ambient conditions. At room temperature coesite becomes the stable phase above 2 GPa, and stishovite above 8 GPa (for the phase boundaries see Akaogi, Navrotsky, 1984). However, at room temperature the low-quartz form is preserved metastably to approximately 15 GPa. Above this pressure it transforms, in a not well understood manner, to an amorphous state (Hemley et al., 1988; Hazen, Finger, Hemley, Mao, 1989; Tattevin et al., 1990).

In recent years crystal-structure investigations have been extended to high pressures, thus complementing high- and low-temperature structure determinations. The literature on the crystal structure and the elastic properties of SiO_2-quartz under ambient and pressure conditions is thoroughly reviewed by Levien, Prewitt and Weidner (1980). A more recent high-pressure structure investigation was performed by Hazen et al. (1989), and a combined high-pressure, high-temperature structural study by Ogata, Takéuchi and Kudoh (1987).

At ambient conditions GeO_2 is stable in the rutile (SiO_2-stishovite) form. Above 1280 K and ambient pressure a low-quartz phase exists which can be flux-grown at lower temperatures and which is quenchable to room temperature. This form is studied here.

The purpose of the present work is to show how both, pressure and chemical variation, affect the low-temperature quartz structure. Furthermore, it should be searched for any crystal-chemical omen for a phase transition under pressure.

Therefore, high-precision high-pressure single-crystal X-ray measurements on SiO_2- and GeO_2-quartz were performed. An earlier study up to 2.5 GPa of the structural behaviour of SiO_2- and GeO_2-quartz was published by Jorgensen (1978), who used time-of-flight neutron powder diffraction.

In addition, the results on quartz-type SiO_2 and GeO_2 are compared with SiO_2-coesite under pressures up to 5.2 GPa (Levien and Prewitt, 1981).

Large parts of the crystal-chemical discussions of this study ground on and extend the ideas of Levien, Prewitt and Weidner (1980) and Levien and Prewitt (1981).

There has been much confusion about the 'proper' space group and choice of the unit cell axes for the low-quartz structure. In this paper the recommendations of Donnay and Le Page (1978) are followed in choosing space group $P3_121$ (No. 152; International Tables, Vol. A, 1989), setting $r(+)$. In this setting the cations occupy the special position $x,0,0$ on the twofold axis parallel [100]. This corresponds to an origin shift of 1/3 **c** compared with International Tables, Vol. A (1989). The reader is directed to Donnay and Le Page (1978) for an extensive discussion of the implications for this setting. The oxygen atoms are in the general position. There are three formula units per unit cell.

Experimental

SiO_2

From a synthetic, untwinned quartz sample (Sawyer Research Products Inc.) (001) wafers of 0.05 and 0.04 mm thickness were cut. Fragments were then broken from these and used in the present study. Sample No. 1 had a triangular shape with edges of 0.10, 0.15, and 0.16 mm and was 0.05 mm

Table 1. Conditions of data collection.

a) SiO_2, quartz

	1st crystal		2nd crystal
Pressure	4.0(1) GPa		10^{-4}, 7.2(1), 10.2(1) GPa
Radiation		MoK_α	
Wavelength		0.71069 Å	
Tube type		fine focus	
Voltage/current		50 kV/40 mA	
$\sin\theta/\lambda$	≤ 1.00 Å^{-1}		≤ 0.90 Å^{-1}
h,k,l		$-10 \leq h,k \leq +10$ $+1 \leq l \leq +10$	
Step-scan type		$2\theta < 30°$: ω-scan $2\theta \geq 30°$: $\omega/2\theta$-scan	
Step width	0.02°		0.015°
Scan velocity	0.01° s^{-1}		0.005° s^{-1}
Scan width per reflection	1.2°		0.9°
No. of reflections	1563		1324, 1137, 1098
No. of reference reflections		3	

b) GeO_2, quartz-type

Pressure	10^{-4} GPa[a]	same crystal at all pressures	1.07(2)[b], 2.18(2)[b], 3.74(2)[b], 4.53(2)[c], 5.12(2)[c], 5.57(2)[c] GPa
Radiation		MoK_α	
Wavelength		0.71069 Å	
Tube type		fine focus	
Voltage/current		50 kV/20 mA	
$\sin\theta/\lambda$	≤ 0.70 Å^{-1}		≤ 1.00 Å^{-1}
h,k,l	$-6 \leq h,k \leq +6$ $0 \leq l \leq +7$		$-6 \leq h,k \leq +6$ $-7 \leq l \leq +7$
Scan type		ω-scan	
Step width		continuous scan	
Scan velocity		variable based on reflection intensity	
Scan width per reflection		1.0°	
No. of reflections	752		742, 727, 754, 523, 519, 518
No. of reference reflections		3	

[a] Data collected for crystal outside diamond cell.
[b] First mounting of crystal.
[c] Second mounting of crystal.

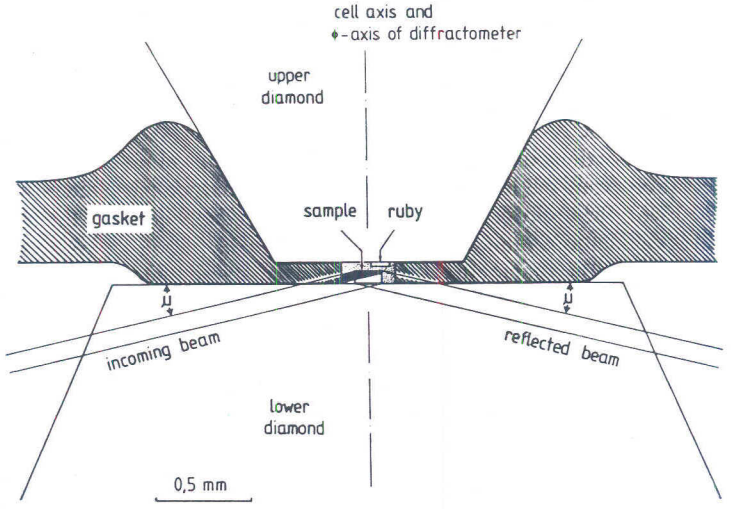

Fig. 1. Basic part of the high-pressure cell used for SiO_2 experiments with diffraction geometry. The shaded area of the incoming beam suffers from increased gasket absorption from inside to outside. The same holds for the reflected beam.

thick. It served only for the 4.0 GPa data sampling (Table 1a) and was broken between the diamonds at the attempt to further increase the pressure. Sample No. 2 was rectangular, 0.14×0.10 mm^2, and 0.04 mm thick. Three data sets, at ambient pressure (10^{-4} GPa), $P = 7.2$ GPa and $P = 10.2$ GPa, were measured from it (Table 1a). The data at 10^{-4} GPa were sampled after release of pressure, still with the crystal mounted within the pressure cell. This provided a measure of the effectiveness of the diamond-cell corrections by comparing the results of the structure refinement at ambient pressure with those from 'normal' ambient-condition experiments. The respective quartz wafer was fixed with its (001) face on the lower diamond (1.9 mm culet; Fig. 1), a small ruby splinter for pressure calibration (Keller and Holzapfel, 1977) on the upper diamond (0.7 mm culet). A 4:1 methanol:ethanol mixture was used as the hydrostatic pressure transmitting medium (Piermarini, Block and Barnett, 1973). The estimated error of the pressure calibration is 0.1 GPa. The gasket was made of INCONEL X750, with a height of 0.10 mm, and a hole of 0.21 mm diameter. A Philips PW1100 four-circle diffractometer equipped with MoK_α radiation and a graphite monochromator was used for the diffraction experiments. Further details are given in Table 1a. Lattice parameters (Table 4a) were calculated from the 2θ angles for always the same 25 reflections in the range $12° \leq 2\theta \leq 67°$. Each reflection was centred in the

four diffractometer settings attainable with the used diamond cell in the bisecting mode (no Friedel reflections possible) (Hamilton, 1974; King and Finger, 1979). Then the average 2θ value with its estimated standard deviation served as input to the lattice-parameter refinement program PARAM of the X-RAY system (Stewart et al., 1972). After refinements with no restrictions on the cell parameters imposed gave no indication of a deviation from the hexagonal lattice, the final lattice parameters were refined with the appropriate constraints. The *Goodness of Fit* of the least-squares calculations ranged between 1.35 and 1.98.

Details of the diamond cell used here and its adaptation to a four-circle diffractometer are described by Koepke (1985), Koepke, Dieterich, Glinnemann and Schulz (1985) and Glinnemann (1987). The cell was first applied to a structure investigation of cordierite up to 2.3 GPa using Beryllium gaskets (Koepke and Schulz, 1986). To extend the pressure range to about 10 GPa, INCONEL X750 gaskets were used in the present study. However, some aspects of the cell especially appropriate to this study should be discussed because they are important in understanding the high quality of the data. There are some salient features of the scattering geometry and sample orientation which contribute to the large volume of reciprocal space which is accessible: In this study between 90 and 93% of all non-Friedel reflections in the chosen range in $\sin\theta/\lambda$, to 1.00 $Å^{-1}$ for the first crystal and to 0.90 $Å^{-1}$ for the second, were measured.

A cross section through the basic part of the cell with an indication of the scattering geometry is given in Fig. 1. The main axis of the cell is perpendicular to the diamond culets, as in the Merrill-Bassett type cell (Merrill and Bassett, 1974). But different from the latter this axis now parallels the ϕ axis of the four-circle diffractometer. The sample is oriented such that its crystallographic main axis **c** coincides with this axis of the cell. This arrangement, in connection with the bisecting mode of the diffractometer, then corresponds to the equi-inclination geometry, where incident and reflected beams for all reflections with a given l index make the same angle with the **c** axis and hence with the gasket (angle μ in Fig. 1). This angle μ ranged from 4° for $hk1$ reflections to 43° for $hk10$ reflections ($hk0$ reflections are completely shadowed by the gasket). Thus, the effective scattering volume of the sample increases from zero at $\mu = 0°$ to a maximum value at maximum μ. In the ideal, rotational-symmetric case of the cell-and-sample arrangement around the ϕ axis, the absorption by the gasket and the lower diamond of all rays for reflections with constant μ, i.e. with constant l index, are the same.

GeO_2

Crystals were grown by a flux technique using a 1:2 molar mixture of LiO_2 and WO_3 as flux (Goodrum, 1972). A small, clear single crystal

($0.12 \times 0.12 \times 0.05$ mm^3) was selected and mounted in a standard fashion on an Enraf-Nonius CAD-4 diffractometer equipped with graphite-monochromatized molybdenum K_α radiation ($\lambda = 0.71069$ Å), and operated by locally-modified CAD-4 software.

Its unit cell was found to be trigonal and the parameters (Table 4b) are in good agreement with those from previous workers (Smith and Isaacs, 1964; Jorgensen, 1978). Intensity measurements were made at ambient conditions through omega scans of those Bragg peaks in the range $0° \leq 2\theta \leq 60°$. Several standard reflections were monitored throughout the data collection and their variations throughout were insignificant.

This crystal was then remounted in a Merrill and Bassett type (Merrill and Basset, 1974) diamond anvil cell. Also placed into the pressure chamber, formed in a 0.25 mm thick stainless steel foil by drilling a 0.35 mm diameter hole, were several small chips of Cr-doped ruby to be used as a pressure calibrant. A mixture of 4:1 methanol:ethanol was used as the hydrostatic pressure transmitting medium. The cell was placed on the diffractometer and the crystal orientation determined through the use of rotation photographs. At this point diffracted-beam measurements of the crystal centering (King and Finger, 1979), locally modified for use with CAD-4 geometry, were used in positioning the cell on the diffractometer. Afterwards this same technique was employed in measuring the "ideal" setting angles for the 12−20 reflections used in refining the crystal orientation and cell parameters. No assumed symmetry was imposed on these refinements, but, up to the highest pressures the lattice remains hexagonal. The intensities of the Bragg peaks were then measured. Locally-modified CAD-4 software was used to measure these reflections in the fixed-phi setting-angle mode (Finger and King, 1978). Within the limited, 82° aperture of the Merrill and Bassett cell all reflections to $2\theta \leq 90°$ were measured. At the end of data collection the pressure was measured through use of the ruby manometer (King and Prewitt, 1980). This sequence was repeated for each pressure listed in Table 1b. This table also summarizes the conditions of the data collection.

In Table 4 are listed some additional, higher pressure, unit cell parameters. A full structure refinement was not performed in this pressure range because a phase transition, which increases the mosaic spread for the crystal and broadens the diffraction peaks, takes place in the interval 5.5 to 6.5 GPa. This will be more fully discussed elsewhere (King, LaPlaca and Dacol, 1990).

Data reduction and structure refinement

SiO_2

Statistical details of the data reduction are found in Table 2a. Conversion of the step-scan data to integral intensities according to Lehmann

Table 2. Statistics of data reduction.

a) SiO_2, quartz

	Pressure/GPa			
	10^{-4} [a]	4.0 [b]	7.2 [a]	10.2 [a]
No. of reflections	1324	1563	1137	1098
$I > 3\sigma(I)$	776 (58%)	628 (40%)	772 (68%)	784 (71%)
After removal of shadowed and falsified reflections	1127	1259	971	942
$I > 3\sigma(I)$	754 (67%)	534 (42%)	753 (78%)	765 (81%)
After averaging	279	337	243	236
$I > 3\sigma(I)$	205 (74%)	218 (65%)	193 (79%)	200 (85%)
Internal R-value for reflections with $I > 3\sigma(I)$	12.7%	16.5%	10.5%	9.8%

b) GeO_2, quartz-type

	Pressure/GPa						
	10^{-4} [c]	1.07(2) [d]	2.18(2) [d]	3.74(2) [d]	4.53(2) [e]	5.12(2) [e]	5.57(2) [e]
No. of reflections	752	742	727	754	523	519	518
After removal of shadowed reflections and those overlapping Be powder diffraction rings	752	433	387	426	391	349	372
$I > 3\sigma(I)$	735	406	352	390	353	314	341

[a] 2nd crystal.
[b] 1st crystal.
[c] Data collected for crystal outside diamond cell.
[d] First mounting of crystal.
[e] Second mounting of crystal.

and Larsen (1974) was performed with the data-reduction part of the PROMETHEUS computing system (Zucker et al., 1983), which also included Lorentz and polarization correction. A maximum of 10% of the measured reflections had to be rejected from each of the data sets due to overlapping with diamond reflections[1] or powder lines from the gasket, as well as partial or complete shadowing by parts of the pressure cell.

The strong absorption of the INCONEL gasket could not be handled analytically. Instead, this problem was treated in two steps. (i) Averaging the intensities of all symmetry-equivalent reflections with given I (six in the case of quartz for a general reflection) helped overcome the asymmetries

[1] The effects of diamond diffraction on the integrated intensities in X-ray single-crystal diamond-anvil cell work has been investigated only very recently by Loveday, McMahon and Nelmes (1990).

Table 3. Goodness of final structure refinements.

a) SiO_2, quartz

	Pressure/GPa			
	10^{-4}	4.0	7.2	10.2
No. of refined parameters	15	15	15	15
$R(\|F\|)/\%$	5.6	9.5	3.8	3.8
$R_w(\|F\|)/\%$	2.3	4.2	2.0	2.1
GOF[a]	2.82	2.31	2.89	3.20

b) GeO_2, quartz-type

	Pressure/GPa						
	10^{-4}[b]	1.07(2)[c]	2.18(2)[c]	3.74(2)[c]	4.53(2)[d]	5.12(2)[d]	5.57(2)[d]
No. of refined parameters	16	16	16	16	16	16	16
$R(\|F\|)/\%$	2.9	2.7	2.5	3.2	2.9	2.6	3.6
$R_w(\|F\|)/\%$	3.8	3.8	3.4	4.7	4.8	3.7	5.1
GOF[e]	0.748	0.707	0.637	0.880	0.890	0.697	0.932

[a] $GOF = \left[\frac{\Sigma w \cdot (|F_o| - |F_c|)^2}{n - m}\right]^{1/2}$ $n - m$ = number of degrees of freedom.

[b] Data collected for crystal outside diamond cell.

[c] First mounting of crystal.

[d] Second mounting of crystal.

[e] $GOF = \frac{[\Sigma w \cdot (|F_o| - |F_c|)^2]^{1/2}}{n - m}$

in the gasket-hole diameter and in the positioning of the non circular crystal within it. These reflections gave reasonable overall internal agreements between 10 and 17% (Table 2a). (ii) To account for the different absorption effects for reflections with different l, separate scale factors were applied to them in the initial steps of the refinements (since $1 \leq l \leq 10$, ten scale factors had to be applied).

Severe extinction is often reported in stuctural studies on quartz (Zachariasen and Plettinger, 1965; Levien, Prewitt and Weidner, 1980; Le Page, Calvert and Gabe, 1980; Kihara, 1990). As a consequence of the just described treatment of absorption, no path lengths of the X-rays inside the sample were available and extinction refinement thus was not possible. On the other hand, a survey of observed and calculated structure factors revealed no indication for extinction. This might be attributed to the fact, that the effective scattering volume for reflections which would suffer most from extinction (small $\sin\theta/\lambda$, small l index) is very small (see end of section Experimental – SiO_2).

The structure refinements were based on $|F|$ values with weights $w = 1/\sigma^2(|F|)$. The estimated standard deviations (e.s.d.'s) of the averaged $|F|$ values of symmetrically equivalent reflections were calculated according to the Gauß error propagation law from the e.s.d.'s of the individual values

Table 4. Results of structure refinements (e.s.d. of least cited figure in parenthesis).

	Pressure/GPa			
	10^{-4}	4.0	7.2	10.2
a) SiO_2, quartz				
a/Å	4.921(1)	4.775(1)	4.6764(8)	4.604(1)
b/Å	5.4163(8)	5.3046(7)	5.2475(5)	5.207(1)
c/a	1.1007(3)	1.1107(5)	1.1221(5)	1.1310(5)
V/Å^3	113.59(4)	104.78(4)	99.38(4)	95.58(4)
Silicon				
x	0.4698(2)	0.4570(5)	0.4503(2)	0.4458(2)
U_{eq} [a]	0.0046(1)	0.0033(4)	0.0050(1)	0.0048(1)
U_{11} [b]	0.0049(3)	0.0012(9)	0.0053(2)	0.0052(2)
U_{22}	0.0041(4)	0.002(1)	0.0041(4)	0.0039(3)
U_{33}	0.0046(2)	0.0069(4)	0.0051(2)	0.0048(2)
U_{23}	0.0002(2)	0.0002(8)	0.0006(2)	0.0006(2)
Oxygen				
x	0.4151(5)	0.408(1)	0.4012(4)	0.3951(4)
y	0.2675(4)	0.2881(9)	0.2971(3)	0.3031(4)
z	−0.1194(1)	−0.1033(4)	−0.0961(2)	−0.0921(2)
U_{eq} [a]	0.0101(3)	0.0108(9)	0.0086(3)	0.0077(2)
U_{11} [b]	0.014(1)	0.017(3)	0.0119(8)	0.0106(7)
U_{22}	0.0102(8)	0.009(2)	0.0082(6)	0.0072(6)
U_{33}	0.0101(4)	0.011(1)	0.0083(3)	0.0076(3)
U_{12}	0.0091(8)	0.010(3)	0.0070(6)	0.0061(5)
U_{13}	0.0029(5)	0.003(2)	0.0026(4)	0.0017(3)
U_{23}	0.0036(4)	0.001(1)	0.0030(3)	0.0020(3)
ϕ/° [c]	16.10(4)	21.7(1)	24.50(7)	26.20(7)

In addition to the above unit cell parameters for GeO_2 the following were determined:
$P = 2.64(2)$ GPa, $a = 4.857(1)$ Å, $c = 5.5925(9)$ Å, $V = 114.27(4)$ Å^3
$P = 3.12(2)$ GPa, $a = 4.8396(9)$ Å, $c = 5.5856(5)$ Å, $V = 113.30(3)$ Å^3
$P = 5.48(2)$ GPa, $a = 4.755(2)$ Å, $c = 5.5505(9)$ Å, $V = 108.67(5)$ Å^3
$P = 6.18(2)$ GPa, $a = 4.726(3)$ Å, $c = 5.537(2)$ Å, $V = 107.1(1)$ Å^3

[a] Given in Å^2; $U_{eq} = \frac{1}{3} \Sigma_i \Sigma_j U_{ij} a_i^* a_j^* \, \mathbf{a}_i \cdot \mathbf{a}_j =$ (for hexagonal axes)

$$= \frac{1}{3} [U_{33} + \frac{4}{3} (U_{11} + U_{22} - U_{12})];$$

its e.s.d. calculated according to Schomaker and Marsh (1983), Eq. (2).

[b] Coefficients U_{ij} of temperature factor T in Å^2; $T = \exp(-2\pi^2 \Sigma_i \Sigma_j U_{ij} h_i h_j a_i^* a_j^*)$.
For Si and Ge only: $U_{12} = 1/2\, U_{22}$, $U_{13} = 1/2\, U_{23}$.

[c] Tetrahedral tilt angle according to Grimm and Dorner (1975).

Table 4. (Continued)

	Pressure/GPa						
	10^{-4}	1.07(2)	2.18(2)	3.74(2)	4.53(2)	5.12(2)	5.57(2)
b) GeO_2, quartz-type							
a/Å	4.9845(2)	4.9288(9)	4.8769(11)	4.8177(13)	4.7883(10)	4.7661(24)	4.7501(1)
c/Å	5.6477(2)	5.6215(10)	5.6007(7)	5.5773(12)	5.5640(6)	5.5534(14)	5.5476(54)
c/a	1.13305(6)	1.1405(3)	1.1484(3)	1.1577(4)	1.1620(3)	1.1652(7)	1.168(1)
V/Å^3	121.506(8)	118.28(4)	115.36(3)	112.08(4)	110.48(3)	109.23(7)	108.39(3)
Germanium							
x	0.45130(6)	0.4479(1)	0.4449(1)	0.4410(1)	0.4392(2)	0.4374(1)	0.4374(2)
U_{eq}[a]	0.0066(1)	0.0079(1)	0.0071(1)	0.0074(2)	0.0074(2)	0.0080(3)	0.0078(3)
U_{11}[b]	0.0073(2)	0.0088(2)	0.0082(2)	0.0084(3)	0.0082(3)	0.0089(3)	0.0087(4)
U_{22}	0.0061(2)	0.0076(2)	0.0069(2)	0.0076(3)	0.0077(4)	0.0081(3)	0.0084(4)
U_{33}	0.0061(4)	0.0071(5)	0.0059(5)	0.0060(7)	0.0061(3)	0.0066(7)	0.0064(9)
U_{23}	0.00043(5)	0.00034(6)	0.00040(7)	0.00026(7)	0.0000(2)	0.0002(1)	−0.0003(1)
Oxygen							
x	0.3965(3)	0.3940(6)	0.3900(6)	0.3873(9)	0.3860(9)	0.3837(8)	0.384(1)
y	0.3022(4)	0.3073(6)	0.3108(7)	0.317(1)	0.320(1)	0.320(1)	0.325(1)
z	−0.0911(3)	−0.0882(5)	−0.0858(5)	−0.0831(8)	−0.0827(7)	−0.0828(6)	−0.0826(8)
U_{eq}[a]	0.0120(4)	0.0128(6)	0.0106(6)	0.012(1)	0.011(1)	0.012(1)	0.012(1)
U_{11}[b]	0.0164(8)	0.017(1)	0.013(1)	0.016(2)	0.015(2)	0.015(2)	0.012(2)
U_{22}	0.0109(8)	0.012(1)	0.009(1)	0.013(2)	0.013(2)	0.013(2)	0.013(2)
U_{33}	0.012(1)	0.012(2)	0.011(2)	0.013(3)	0.007(1)	0.010(3)	0.013(4)
U_{12}	0.0090(4)	0.0092(7)	0.0063(6)	0.011(1)	0.009(1)	0.0094(7)	0.0084(9)
U_{13}	0.0057(9)	0.006(1)	0.004(1)	0.003(2)	0.0031(9)	0.004(2)	0.004(2)
U_{23}	0.0049(6)	0.0052(7)	0.0042(6)	0.005(1)	0.004(1)	0.004(1)	0.005(1)
ϕ/°[c]	26.50(6)	27.7(2)	28.8(2)	30.0(2)	30.3(2)	30.5(2)	30.6(2)

or from the dispersion of the single measurements (Zucker et al., 1983). The respective greater value was used as the e.s.d. of a unique reflection. The error of a single measurement was deduced from counting statistics.

Structure refinements were carried out with the X-RAY system (Stewart et al., 1972) using only $|F| > 3\sigma(|F|)$ and atomic form factors of neutral atoms (Cromer and Mann, 1968). Each reciprocal-lattice layer with l constant received its own scale factor (see above). In the initial stages of refinement with isotropic temperature factors each scale factor was treated independently. The l dependence of the scaling was then fixed and the refinements continued by including anisotropic thermal motion parameters

Table 5. Atomic distances and bond angles (e.s.d. of least cited figure in parenthesis).

	Pressure/GPa			
	10^{-4}	4.0	7.2	10.2
a) SiO_2, quartz				
d(Si–O)/Å				
2 × Si–O (*d*1)	1.614(2)	1.613(4)	1.615(1)	1.614(1)
2 × Si–O (*d*2)				
⟨Si–O⟩[a]	1.610(2) (1)	1.608(5) (3)	1.6070(15) (8)	1.6066(15) (8)
Tetrahedral edges, $d(O\ldots O)_T$/Å				
2 × O…O (*A*)	2.640(3)	2.651(6)	2.672(2)	2.690(2)
2 × O…O (*B*)	2.615(3)	2.593(8)	2.580(3)	2.569(2)
1 × O…O (*C*)	2.637(2)	2.635(5)	2.629(2)	2.617(2)
1 × O…O (*D*)	2.621(2)	2.623(5)	2.609(2)	2.601(2)
⟨O…O⟩[a]	2.628(3) (1)	2.626(6) (3)	2.6237(23) (9)	2.6227(20) (8)
Tetrahedral angles, (O–Si–O)/°				
2 × O–Si–O (α)	110.19(7)	111.1(2)	112.49(6)	113.72(5)
2 × O–Si–O (β)	108.69(7)	107.6(2)	106.80(6)	106.20(5)
1 × O–Si–O (γ)	109.6(1)	109.6(3)	108.97(9)	108.37(9)
1 × O–Si–O (δ)	109.5(1)	109.9(3)	109.37(9)	109.80(9)
⟨O–Si–O⟩[a]	109.48(8) (3)	109.5(2) (1)	109.49(7) (3)	109.50(6) (3)
Tetrahedral volume, V_T/Å^3[b]	2.139	2.128	2.124	2.118
Angle at bridging oxygen, (Si–O–Si)/[c]				
4 × Si–O–Si	144.2(2)	137.1(4)	133.1(1)	130.3(1)
Distance of tetrahedral centres, d(Si…Si)/Å				
4 × Si…Si	3.0627(4)	2.992(2)	2.9477(9)	2.9152(8)
Oxygen-oxygen distances between tetrahedra, d(O…O)/Å				
2 × O…O (*D*1)	3.414(2)	3.158(7)	3.031(2)	2.947(2)
1 × O…O (*D*2)	3.345(2)	3.033(4)	2.884(2)	2.793(2)

Table 5. (Continued)

	Pressure/GPa						
	10^{-4}	1.07	2.18	3.74	4.53	5.12	5.57
b) GeO_2, quartz-type							
d(Ge−O)/Å							
2 × Ge−O (*d*1)	1.739(2)	1.738(3)	1.741(3)	1.740(4)	1.734(4)	1.735(3)	1.724(4)
2 × Ge−O (*d*2)	1.738(2)	1.736(3)	1.734(3)	1.734(4)	1.737(4)	1.731(4)	1.745(5)
⟨Ge−O⟩[a]	1.738(2) (1)	1.737(3) (2)	1.737(4) (3)	1.737(4) (3)	1.736(4) (3)	1.733(4) (3)	1.734(5) (3)
Tetrahedral edges, d(O…O)$_T$/Å							
2 × O…O (*A*)	2.903(2)	2.909(3)	2.922(3)	2.930(4)	2.935(5)	2.940(4)	2.943(5)
2 × O…O (*B*)	2.782(1)	2.770(2)	2.762(2)	2.749(4)	2.738(3)	2.733(3)	2.725(4)
2 × O…O (*C*)	2.855(3)	2.854(6)	2.853(6)	2.853(8)	2.841(7)	2.831(7)	2.824(9)
2 × O…O (*D*)	2.804(3)	2.804(5)	2.795(5)	2.802(8)	2.811(8)	2.799(8)	2.825(10)
⟨O…O⟩[a]	2.836(2) (1)	2.835(4) (2)	2.833(4) (2)	2.834(5) (2)	2.833(5) (2)	2.829(5) (2)	2.831(6) (3)
Tetrahedral angles, (O−Ge−O)/°							
2 × O−Ge−O (α)	113.24(8)	113.7(1)	114.5(1)	115.0(2)	115.5(2)	116.0(2)	116.1(2)
2 × O−Ge−O (β)	106.28(4)	105.74(6)	105.31(7)	104.6(1)	104.1(1)	104.1(1)	103.5(1)
1 × O−Ge−O (γ)	110.3(1)	110.3(2)	110.0(2)	110.1(3)	110.0(3)	109.3(3)	110.0(3)
1 × O−Ge−O (δ)	107.6(1)	107.8(2)	107.5(2)	107.8(2)	108.0(2)	107.9(2)	108.1(3)
⟨O−Ge−O⟩[a]	109.49(7) (3)	109.50(13) (5)	109.51(13) (6)	109.52(19) (8)	109.53(20) (8)	109.54(13) (6)	109.6(2) (1)
Tetrahedral volume, V_T/Å^3[b]	2.686	2.677	2.672	2.667	2.656	2.642	2.647

Table 5. (Continued)

	Pressure/GPa						
	10^{-4}	1.07	2.18	3.74	4.53	5.12	5.57
Angle at bridging oxygen, (Ge−O−Ge)/°							
4 × Ge−O−Ge	130.04(9)	128.4(2)	126.8(2)	125.0(2)	124.3(2)	124.0(2)	123.4(3)
Distance of tetrahedral centres, d(Ge...Ge)/Å							
4 × Ge...Ge	3.1515(3)	3.1277(5)	3.1061(5)	3.0824(5)	3.0702(8)	3.0614(5)	3.054(1)
Oxygen−oxygen distances between tetrahedra, d(O...O)/Å							
2 × O...O ($D1$)	3.192(2)	3.125(4)	3.070(4)	2.999(6)	2.967(5)	2.954(5)	2.926(6)
1 × O...O ($D2$)	3.023(3)	2.959(6)	2.906(6)	2.847(9)	2.828(8)	2.820(7)	2.809(9)

[a] E.s.d. of mean values, see main section Data reduction and structure refinements, Eqs. (1) and (2).

[b] Tetrahedral volume V_T:

$$V_T^2 = \frac{1}{288} \det \begin{pmatrix} 0 & A^2 & B^2 & C^2 & 1 \\ & 0 & D^2 & B^2 & 1 \\ & & 0 & A^2 & 1 \\ & & & 0 & 1 \\ & & & & 0 \end{pmatrix}, \text{ with } A \text{ to } D \text{ tetrahedral edges.}$$

and a single, overall scale factor. Refinements in which the scale factors were allowed to vary had indicated unacceptable correlations with some of the anisotropic thermal motion parameters.

Mechanical stress can induce twinning in a quartz crystal. Such stress can occur during sample preparation and/or from non-hydrostatic conditions during the pressure experiment. For that reason all refinements were carried out with variable twin portions (Zachariasen and Plettinger, 1965), but no twinning was observed. Table 3a shows the quality of the final refinements in terms of *R*-values and *Goodness of Fit*; in Table 4a the results are listed.

The high percentage of accessible reflections along with the effectiveness of the 'corrections' for absorption are reflected in the high precision of the results (Tables 2a–5a): They are in excellent agreement with previous ambient-pressure studies (Young and Post, 1962; Smith and Alexander, 1963; Zachariasen and Plettinger, 1965; Le Page and Donnay, 1976; Le Page, Calvert and Gabe, 1980; Levien, Prewitt and Weidner, 1980; Wright and Lehmann, 1981; Lager, Jorgensen and Rotella, 1982; Will, Parrish and Huang, 1983; Ogata, Takéuchi and Kudoh, 1987; Hazen et al., 1989; Kihara, 1990), and the high-pressure results have higher precision than those from any other previous high-pressure study (Jorgensen, 1978; D'Amour, Denner and Schulz, 1979; Levien, Prewitt and Weidner, 1980; Ogata, Takéuchi and Kudoh, 1987; Hazen et al., 1989).

Table 5a gives atomic distances and bond angles as calculated with the program BONDLA of the X-RAY system (Stewart et al., 1972). For mean values, two kinds of estimated standard deviations are given in parentheses,

$$\sigma_1 = 1/n \cdot \Sigma\sigma_i \text{ and} \tag{1}$$

$$\sigma_2 = 1/n \cdot \sqrt{\Sigma\sigma_i^2}\,. \tag{2}$$

σ_1 gives an upper limit, σ_2 a lower limit of the correct standard deviation (Hazen and Finger, 1982, p. 84/85).

GeO_2

The scan profile data were reduced to integrated intensities by dividing the scan into three segments. The left and right segments were used in calculating an average background which was then subtracted from the intensity value obtained in a numerical integration of the central, peak region. Corrections were then applied for crystal absorption, Lorentz effect, and incident X-ray polarization. In addition to the corrections applied to the ambient-condition data, the high-pressure data were corrected for the diamond-cell absorption in a manner similar to that described in Finger and King (1978). Also, those reflections overlapping the beryllium powder-diffraction rings and those outside the 82° aperture of the cell were elimin-

ated. This is summarized in Table 2b. In a few instances overlap with diamond reflections biased a reflection and these reflections were removed from the data. Approximately, one reflection for each data set was affected by this.

The structure refinements were based on $|F|$ values with weights, $w = 1/\sigma^2(|F|)$, where σ was estimated from counting statistics. Structure refinements were carried out with a locally modified version of the program ORFELS (Busing, Martin and Levy, 1964), using only $|F| > 3\sigma(|F|)$ and atomic form factors of neutral atoms (Cromer and Mann, 1968).

The results for the ambient-pressure structure, Table 4b, are in excellent agreement with previous studies (Smith and Isaacs, 1964; Jorgensen, 1978).

Atomic distances and bond angles (Table 5b) were calculated with the program ORFFE. For the two types of standard deviations given for mean values in Table 5b see Eqs. (1) and (2).

Results and discussion

Unit cell compression

Both SiO_2 and GeO_2 are highly compressible when compared to most oxides. The previously obtained values for SiO_2 for the bulk modulus (i.e. the reciprocal of the volume compressibility), $K_0 = 37.1(2)$ GPa, and its pressure derivative, $K'_0 = 6.2(1)$ (Levien, Prewitt and Weidner, 1980) and $K_0 = 34(4)$ GPa, $K'_0 = 5.7(9)$ (Hazen et al., 1989) are in good agreement with the compression found here (Fig. 2). The unit cell volumes for GeO_2 in Table 4b were used in a least-squares fit to the Birch-Murnaghan equation of state and the resulting values are $K_0 = 39.2(4)$ GPa and $K'_0 = 3.8(4)$. (The equation of state and the fitting procedure are described by Bass, Liebermann, Weidner and Finch, 1981.) This K_0 value is in excellent agreement with that obtained by Jorgensen (1978), but his K'_0 value is nearly a factor of two smaller. However, the accuracy in determining K'_0, which describes the curvature of the P–V data, is very sensitive to the pressure range of the experimental data. The threefold increase in range for the present study over that of Jorgensen (1978) makes it likely the new value is a better estimate. The quite different bulk modulus for coesite, $K_0 = 96(3)$ GPa (Levien and Prewitt, 1981) shows that this silica polymorph is much less compressible than both quartz phases.

As can be seen from comparison of the SiO_2 and GeO_2 values for K_0, and also from Fig. 2, the volume compressibility for these two crystals is nearly equal. However, Fig. 3 shows that the anisotropy of the cell dimensions, measured by the c/a ratio, is quite different for the two. At ambient pressure the c/a ratio for GeO_2 is much larger than that for SiO_2, an indication of the increased distortion of the tetrahedra in the former crystal

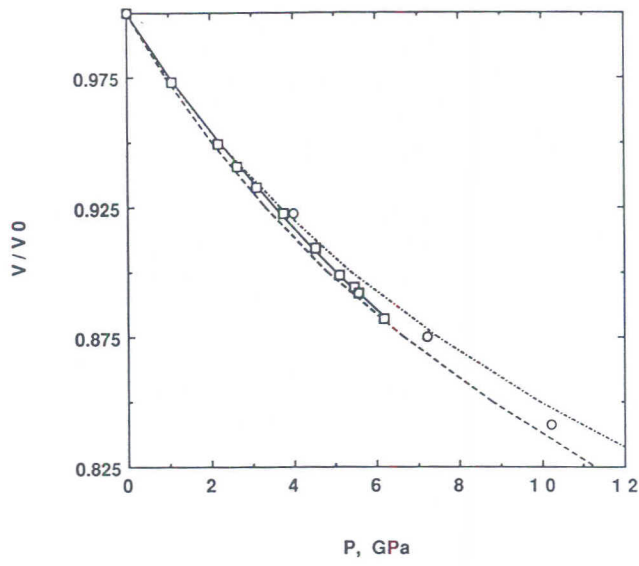

Fig. 2. Volume compression for GeO_2 (□) and SiO_2 (○). The solid line is a least-squares fit to a Birch-Murnaghan equation of state (see text under Unit cell compression). The dashed lines are published fits to a Birch-Murnaghan equation of state for SiO_2: –·–·– Levien, Prewitt, Weidner (1980) and – – – – Hazen et al. (1989).

(Smith, 1963; Smith and Isaacs, 1964; Megaw, 1973, pp. 453–459; Grimm and Dorner, 1975). Increasing pressure causes the *c*/*a* ratios for both compounds to increase, but the rate for GeO_2 is nearly twice that of SiO_2. The tetrahedral distortions implied by this difference are discussed in the section Intra-tetrahedral features: General. The nearly equal volume compressibility for the two compounds implies that the variation of the product of the *c* and *a* parameters is nearly equal for the two structures. Therefore the strong difference in the pressure derivative of the *c*/*a* ratio must derive from a coupled difference in the compressibility of the **a** and **c** axes. Indeed, the **a**-axis compressibility for SiO_2 is found to be about 20% less than that for GeO_2, whereas the **c**-axis compressibility is about 25% greater. This should be reflected in quite different elastic constants for the two materials, but those for quartz-like GeO_2 have not been measured.

In Fig. 4 the *c*/*a* ratio is plotted against the unit-cell volume (normalized to ambient conditions). The SiO_2 data include high-pressure, room-temperature studies as well as low- and high-temperature, ambient pressure ones. There is clearly a break in slope at ambient volume indicating a

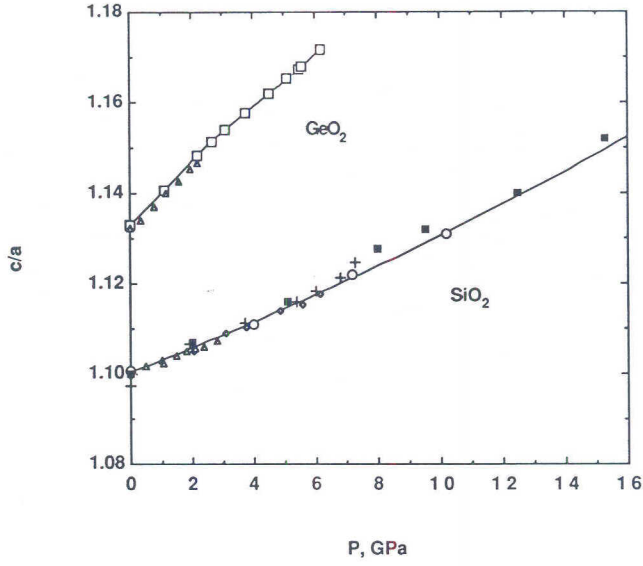

Fig. 3. Ratio of hexagonal unit-cell axes, c/a, as a function of pressure. ○, □ this study; △ Jorgensen (1978); + D'Amour et al. (1979); ◇ Levien et al. (1980); ■ Hazen et al. (1989).

difference between pressure- and temperature-induced tetrahedral distortions (see last main section Brief comparison ...).

For an elucidation of the high compressibility and its anisotropy in the c and a parameters details of the crystal structures under pressure have to be discussed.

Thermal displacement parameters

SiO_2

Anisotropic thermal displacement parameters were refined at each pressure, and the U_{ij} values are given in Table 4a. The magnitudes of the ambient-pressure values are in general agreement with those given by previous authors [cf. Kihara (1990) for a discussion of the differences in these values found in the literature]. An analysis of the RMS magnitudes of the eigen values from the thermal-motion tensors show similar good agreement. The silicon atom is essentially isotropic whereas the oxygen atoms exhibits significant anisotropy, with 60 percent difference between the maximum and minimum RMS displacement. Previous studies have shown that this

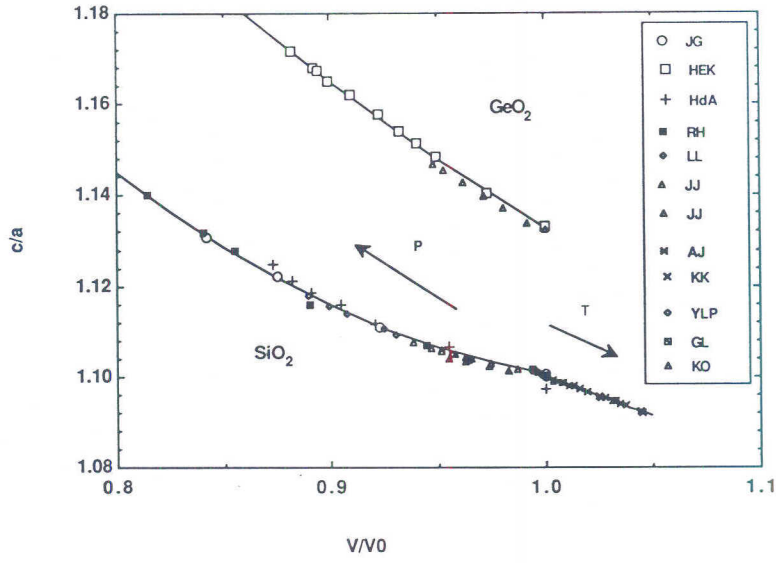

Fig. 4. Ratio of hexagonal unit-cell axes, c/a, as a function of normalized cell volume, V/V_0, with V_0 the unit-cell volume at ambient conditions. The high- and low-temperature data are seen to follow a distinctly different trend than that found at high pressure. The legend for this figure is followed throughout the other figures and is as follows: JG, SiO_2 – this study; HEK, GeO_2 – this study; HdA, D'Amour et al. (1979); RH, Hazen et al. (1989); LL, Levien, Prewitt and Weidner (1980); JJ, Jorgensen (1978); AJ, Jay (1933); KK, Kihara (1990), YLP, Le Page, Calvert and Gabe (1980); GL, Lager, Jorgensen and Rotella (1982); KO, Ogata et al. (1987).

maximum is nearly perpendicular to the plane formed by the Si–O–Si linkage [cf. Kihara (1990) for a discussion], but the orientation found here is at an arbitrary angle to this plane. The high-pressure refinements exhibit additional, different orientations. This probably is an artifact of the correlation between the thermal parameters and the angle-dependent scale factors used in correcting the diamond cell absorption (see Data reduction and structure refinement). However, this is apparently a small effect, and as pressure is increased the expected slight reduction in magnitude of the oxygen thermal motion is observed (see for example U_{eq} in Table 4a).

GeO_2

Anisotropic thermal displacement parameters were also refined for these data and the values are given in Table 4b. The eigen values from the displacement tensor show that the germanium atom is essentially isotropic

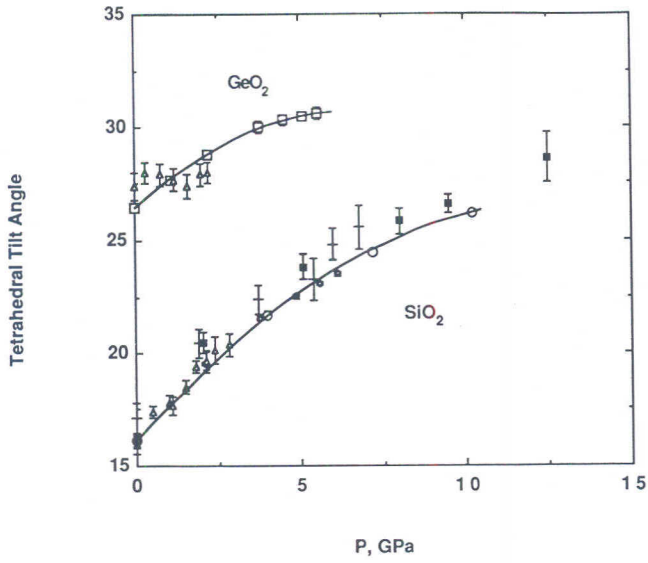

Fig. 5. Inter-tetrahedron distortion parameter (tilt angle ϕ, see Grimm and Dorner, 1975) increases with pressure but begins to saturate at the highest pressures. At 10 GPa the magnitude for the tilt in SiO_2 equals that in GeO_2 at ambient pressure. Data shown are (see Fig. 4 for legend): JG, HEK, HdA, JJ, LL, and RH.

at all pressures whereas the oxygen atom is highly anisotropic. The degree of anisotropy equals that noted above for oxygen in SiO_2. The orientation for this large oxygen displacement is perpendicular ($5 \pm 5°$) to the plane formed by the Ge–O–Ge inter-tetrahedron linkage. In contrast to SiO_2, for neither atom in GeO_2 can a significant change with pressure be resolved: The U_{eq} values in Table 4b are nearly constant. This undoubtedly reflects the much greater range of compression measured for SiO_2 than for GeO_2. The orientation of the oxygen atom displacement are also unchanged at high pressures. The ambient pressure results reported here are in excellent agreement with those of Smith and Isaacs (1964) on GeO_2.

Inter-tetrahedal features: General

Thermal expansion and baric compression (at least in the investigated pressure ranges) are mainly accomplished by rotation of the tetrahedra around their twofold axes. In the idealized high-quartz structure this "tilt angle (ϕ)" is zero. (For the calculation of this angle and related topics, as atomic parameters and lattice constants for structure models of quartz with

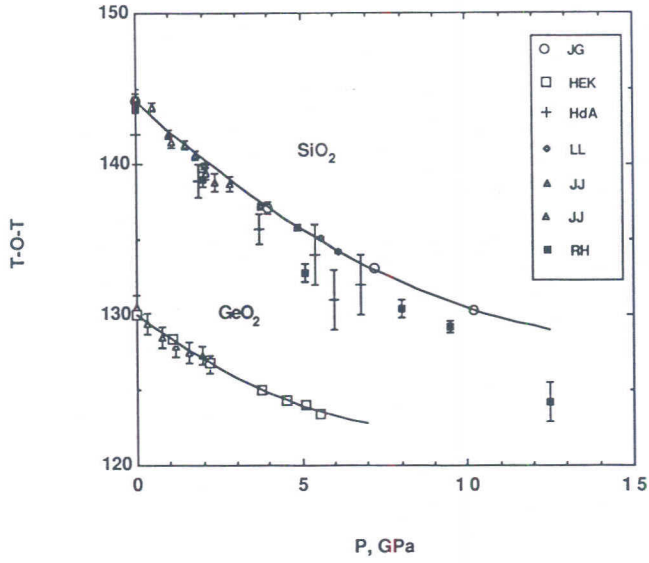

Fig. 6. Inter-tetrahedron T–O–T angle decreases with pressure for both materials. At 10 GPa the magnitude of Si–O–Si equals that for Ge–O–Ge at ambient pressure. (See Fig. 4 for legend.)

given tetrahedra but different tilt angle, see Grimm and Dorner, 1975.) It increases to about 16° for low-quartz at room temperature and ambient pressure. Its further increase with pressure is given in Table 4 and is shown in Fig. 5. For both compounds, SiO_2 and GeO_2, the rate of tilting decreases with increasing pressure, the tilt angles apparently reaching maxima slightly above 14 GPa (SiO_2) and 7 GPa (GeO_2). The tilting of the tetrahedra accounts for 13% of the total 16% in volume decrease for quartz, and for 8% of the total 11% for GeO_2. (Here the unit-cell volumes of structural models built from ambient-pressure tetrahedra tilted to the maximum experimental angles were compared with the experimental unit-cell volumes.) The tilting is correlated with a pronounced decrease in the T–O–T angle (Table 5, Fig. 6), in GeO_2 less so than in quartz for the same pressure range. In quartz the T–O–T angle reaches 130° at 10 GPa, the value in GeO_2 for ambient conditions (as also observed for the tilt angle ϕ). In GeO_2 it decreases further to 123°. Under ambient conditions the T–O–T angle varies between ca. 120 and 180° in silicates (Liebau, 1985, p. 16) and between 110 and 136° in germanates (Hill, Louisnathan and Gibbs, 1977). Thus no peculiarity can be seen in the values found in the investigated pressure ranges.

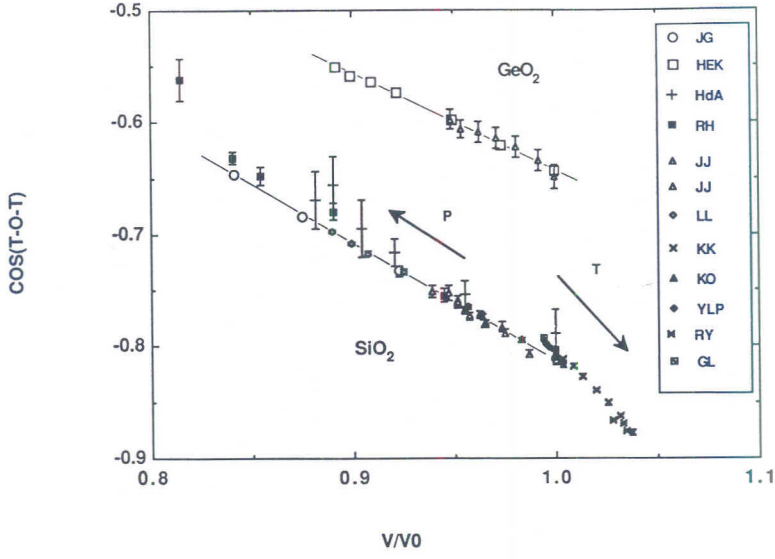

Fig. 7. Cos(T−O−T) vs. V/V_0. A linear scaling of cos(T−O−T) with respect to normalized volume, V/V_0, is found for the high-pressure data, but the temperature data lay along a different trend. [See Fig. 4 for legend except RY, Young (1962).]

Figures 5 and 6 clearly demonstrate the higher precision of the structural data of Levien, Prewitt and Weidner (1980) and of this work as compared to the other authors. This will also become apparent from Figs. 7 to 9.

The correlation between cell volume and T−O−T angle is shown in Fig. 7. [The choice of cos<(T−O−T) serves only to show the linear relationships; a structural explanation for this linearity is not known to the authors.] In both quartz-type phases the pressure dependent variation is similar, as the two nearly parallel lines clearly indicate. (For the different slope of the temperature dependence in quartz see last main section Brief comparison...)

Decrease of the T−O−T angle results in shortening of the T...T distance. At the maximum pressures this quantity, 2.92 Å for SiO_2 and 3.05 Å for GeO_2 (Table 5), falls slightly below the reported smallest values for silicates and germanates under ambient conditions, 2.94 and 3.06 Å, respectively (O'Keeffe and Hyde, 1978; Hill, Louisnathan and Gibbs, 1977).

The decrease of the two shortest inter-tetrahedral O...O distances with pressure in both compounds is shown in Fig. 8A and B. The shortest one (*D2*), 2.79 Å for SiO_2 and 2.81 Å for GeO_2 respectively, at highest pressures, are still longer than the shortest reported lengths in silicates (2.75 Å in

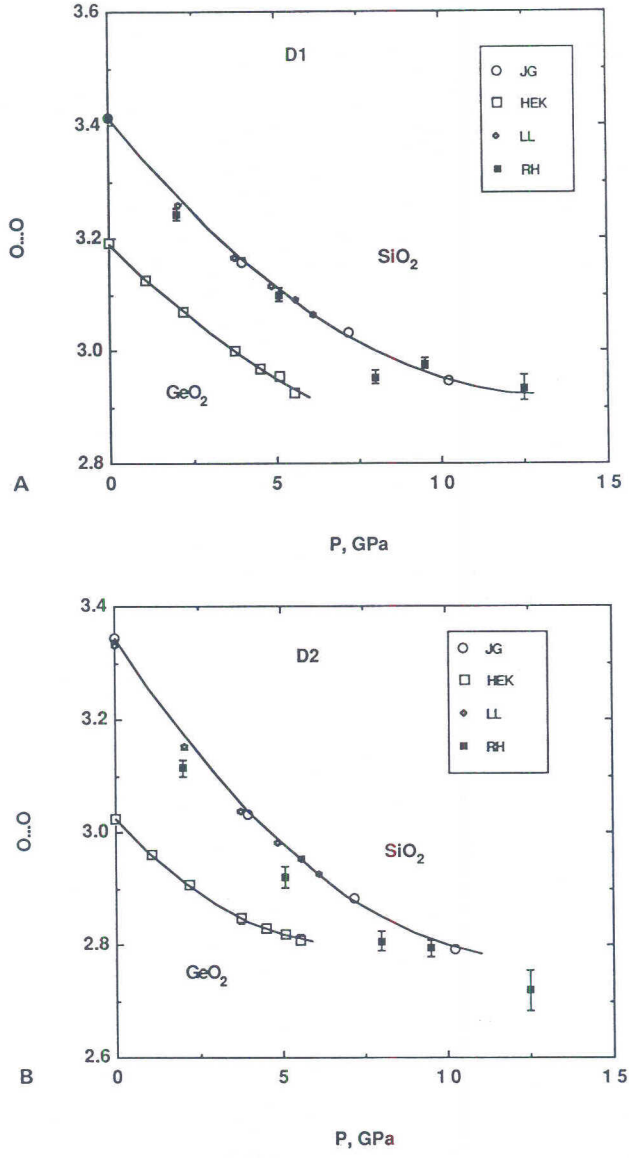

Fig. 8A, B. Inter-tetrahedron oxygen-oxygen distances O...O as function of pressure. For GeO_2 the *D*2 distance becomes shorter than several intra-tetrahedron distances for $P > 2$ GPa. Where no error bars are given, they are smaller than symbols. (See Fig. 4 for legend.)

phenacite; Zemann, 1986) and in oxide structures (2.65 Å for UTe_3O_9; Zemann, 1986).

In a structural model with tilted, but regular tetrahedra, where the tilt angle is the experimental value and the T–O distance the mean of the experimental values, both at highest pressure, the shortest inter-tetrahedral O...O distance *D*2 would be reduced to 2.65 Å for quartz and 2.55 Å for GeO_2. In these models the unit-cell volume is always greater than the experimental one. If one chooses the experimental volume, the tilt angle ϕ in the models has to be larger which would lead to even shorter oxygen-oxygen distances. Thus, it is the progressive tetrahedral distortion (see section Intra-tetrahedral features: General) with pressure which prevents this O...O distance *D*2 from becoming unusually small in the pressure ranges investigated. The reverse holds for the T...T distance; in the models it is larger than the experimental value. Both observations together indicate that inter-tetrahedral O...O interactions are more important than T...T repulsions. This is similar to the conclusions drawn by Levien, Prewitt and Weidner (1980), but is in disagreement with those of O'Keeffe and Hyde (1978, 1981). Furthermore, the model of rigid regular tetrahedra leads to a reduction of c/a with pressure (1.054 for SiO_2 and 1.037 for GeO_2 at highest pressures), whereas in reality the reverse is observed (Table 4, Fig. 3 and 4). This can be understood in terms of oxygen-oxygen repulsions: The shortest O...O vector, *D*2, has a larger component parallel to **c** than perpendicular to it.

For SiO_2 both inter-tetrahedral O...O distances *D*1 and *D*2 remain larger than any of the tetrahedral edges. For GeO_2, however, above ca. 2 GPa *D*2 becomes shorter than the two longest tetrahedral edges (*A*, Table 5b). At maximum pressure only the two shortest tetrahedral edges (*B*) are shorter than *D*2, whilst even *D*1 becomes smaller than the edges (*A*). Thus, oxygen changes its coordination number from six to nine in the investigated pressure range (concerning only the anions). Sowa (1988) investigated the changes in the anion packing of the quartz structures of SiO_2 and GeO_2 under pressure by calculating and visualizing the Dirichlet domains (Wirkungsbereiche) of the oxygen atoms by ignoring the cations. The oxygen packing becomes more and more regular. The atoms 'moving' on paths as, when extrapolated, to finally reach positions at the lattice points of a cubic body-centred lattice. On that way, on the other hand, the $(Si,Ge)O_4$ tetrahedra would distort so heavily as the cations could not tolerate, thus making a phase transition probable (Sowa, 1988).

Inter-tetrahedral features: Correlations

In the literature numerous correlations are discussed between crystal-chemical quantities in structures with tetrahedral building units (Baur, 1970; Louisnathan and Gibbs, 1972; Hill, Louisnathan and Gibbs, 1977; Hill

and Gibbs, 1979; Baur and Ohta, 1982; Geisinger, Gibbs and Navrotsky, 1985; Liebau, 1985; pp. 22–24). Except those of Liebau (1985, pp. 22–24) they apply to many different structures at ambient conditions, but not to variations of the same structure under elevated pressures or changing temperatures. Most of these correlations do not hold for the two quartz-type compounds and for coesite under pressure. Three of them, showing at least some qualitative agreements are:

(i) A number of regressions show a shortening of the T–O bonds with increasing T–O–T angles. In coesite this relation holds qualitatively between the different angles at constant pressure (Levien and Prewitt, 1981). The variation with pressure in the individual angles, however, does not follow this trend: The T–O–T angles in all three compounds, coesite, quartz and quartz-type GeO_2, decrease under pressure, but the T–O distances are essentially constant. This behaviour agrees with a molecular orbital study under simulated compression (Ross and Meagher, 1984).

(ii) In silica polymorphs under ambient conditions a strong correlation exists between the T–O–T angle and the T...T distance, which can be described by the following equation (Hill and Gibbs, 1979):

$$\log\left\{\sin\frac{1}{2}(\mathrm{T-O-T})\right\} = a + b\cdot\log\{d(\mathrm{T...T})\}. \tag{3}$$

Here b equals 1 and $a = \log\{2\langle d(\mathrm{T-O})\rangle\}$, $\langle d(\mathrm{T-O})\rangle$ being the average of the two T–O bonds in the T–O–T group. For the quarz phases under pressure the experimental data yield:

$$\log\left\{\sin\frac{1}{2}(\mathrm{Si-O-Si})\right\} = -0.47 + 0.93\cdot\log\{d(\mathrm{Si...Si})\} \tag{4}$$

($N = 17$, $r = 0.98$) and

$$\log\left\{\sin\frac{1}{2}(\mathrm{Ge-O-Ge})\right\} = -0.50 + 0.92\cdot\log\{d(\mathrm{Ge...Ge})\} \tag{5}$$

($N = 14$, $r = 0.98$, with N the number of observations and r the linear regression coefficient).

These relations, together with the experimental data points, are plotted in Fig. 9, where also the temperature dependence of the respective quantities in SiO_2-quartz is shown. The dashed lines in Fig. 9 represent Eq. (3) with constant $\langle d(\mathrm{T-O})\rangle$ values[2], i.e. a model with hard-sphere T atoms riding without constraints on hardsphere oxygen atoms. If nonbonded cation–cation repulsions are assumed to be mainly responsible for structural details

[2] The values used here, $\langle d(\mathrm{Si-O})\rangle = 1.61$ Å, $\langle d(\mathrm{Ge-O})\rangle = 1.74$ Å, are the mean bond lengths at ambient conditions, cf. Table 5.

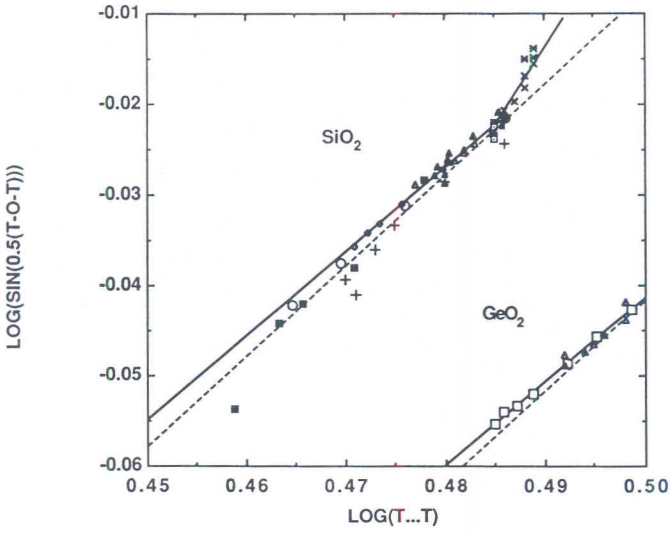

Fig. 9. Linear relation between inter-tetrahedron T−O−T angle and T...T distance as described by Hill and Gibbs (1979) (see Eqs. 3 to 5). Solid lines are best fits to the experimental data. For SiO_2 high-pressure data only from JG and LL were used (others ignored according to low precision), ambient-conditions data from JG, LL, GL, YLP, JJ, KK, KO and RY (N = 17; see Eq. 4). Dashed lines are calculated with the mean T−O distances at ambient conditions. The high- and low-temperature data deviate from the trend seen in the high-pressure data. (See Figs. 4 and 7 for legend.)

under pressure, one would expect the experimental data to lie *below* this dotted line for the hard-sphere model, because shorter d(T...T) values would imply larger T−O distances (O'Keeffe and Hyde, 1978, 1981). The four variable Si−O−Si groups in coesite follow no uniform trend (Levien and Prewitt, 1981).

(iii) According to Liebau (1985, pp. 29/30) larger individual and mean isotropic atomic displacement parameters of the bridging oxygen atoms correlate with larger individual and mean Si−O−Si angles. For SiO_2-quartz under pressure U_{eq}(O) and the Si−O−Si angle follow this trend qualitatively. For coesite under pressure there is a qualitative agreement only in the mean values. There is no significant trend in U_{eq}(O) for GeO_2 in the investigated pressure range.

Intra-tetrahedral features: General

The TO_4 tetrahedra remain nearly unchanged within the relatively large error limits in the pressure studies of Jorgensen (1978) and D'Amour,

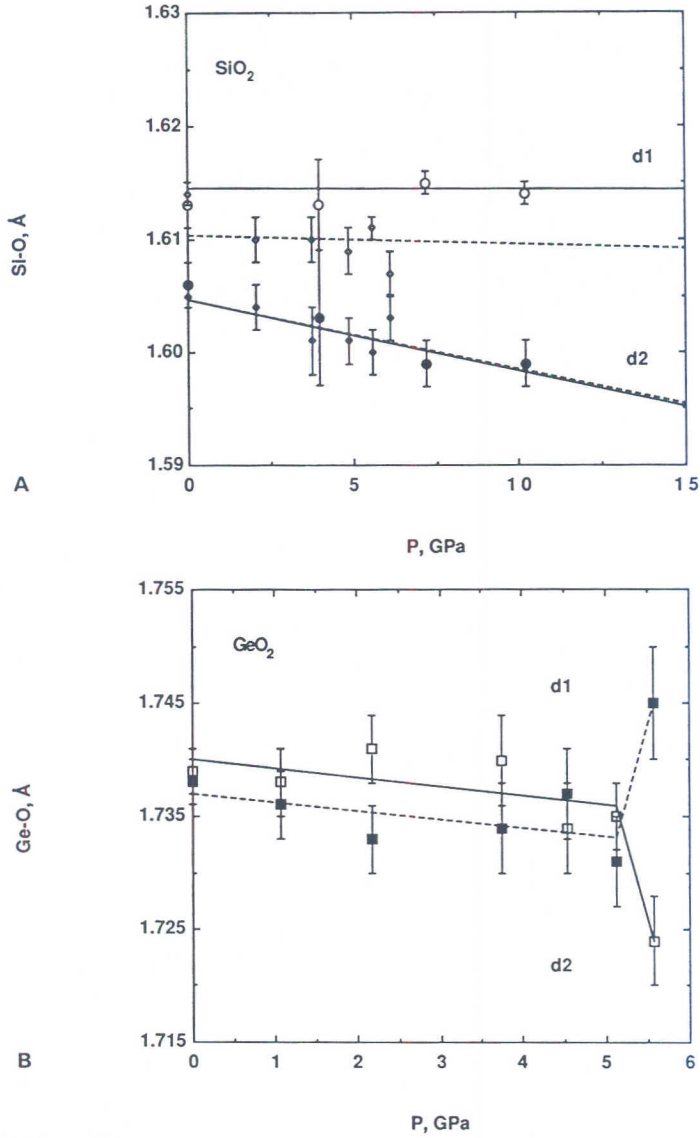

Fig. 10A, B. Variation of the two independent T−O distances with pressure. Straight lines are weighted least-squares lines. SiO_2: ○, ● this study; ◇, ◆ Levien, Prewitt and Weidner (1980), for the fitted lines data at ambient conditions are omitted; GeO_2: this study.

Denner and Schulz (1979). However, the increase in the c/a ratio with pressure, already observed by these authors (Fig. 3 and 4), indicate progressive tetrahedral distortion (Smith, 1963; Smith and Isaacs, 1964; Megaw, 1973, pp. 453–459; Grimm and Dorner, 1975). The higher precision of the work of Levien, Prewitt and Weidner (1980) and of the present study, however, allows one to resolve also intra-tetrahedral changes. The work of Hazen et al. (1989) on quartz-SiO_2 is of intermediate precision, individual T–O distances are not well determined, but the trend in the overall distortion of the SiO_4 tetrahedron is correct.

For SiO_2 the larger of the two Si–O distances remains constant (Table 5a, Fig. 10A), whereas the shorter one decreases slightly. The actual values for the larger distance ($d1$) are slightly different in this study compared to Levien, Prewitt and Weidner (1980), except at ambient conditions. The values measured here were all determined from data taken on the crystal mounted in the diamond cell, even those at ambient pressure (see section Experimental). This is not the situation for the ambient-pressure data of Levien, Prewitt and Weidner (1980) which were collected with the crystal *not loaded* in the high-pressure cell. Perhaps there is a slight ($\approx 2\sigma$) systematic bias in their high-pressure values for $d1$. For comparison, in coesite the changes in the individual and mean Si–O lengths up to 5.2 GPa are larger than in quartz up to 10 GPa.

The changes in the two Ge–O bond lengths are less regular than those for Si–O (Fig. 10B). At ambient pressure the two values are nearly equal, in good agreement with Smith and Isaacs (1964). With increasing pressure one can see that there is smooth variation but no general trend except at the highest pressure point, 5.6 GPa, where there is a sudden divergence of the values. This may be related to the phase transformation which is found at a slightly higher pressure (see section Experimental).

As already discussed by Levien, Prewitt and Weidner (1980) for quartz, the tetrahedral distortion increases with pressure. This holds also for GeO_2. Furthermore, the distortions are very similar in both compounds: The differences between the largest (A) and shortest (B) edges increase; the same holds for the largest (α) and smallest (β) angles (Table 5). Moreover, the O–T–O angles in quartz vary in such a way that at 10 GPa the values for GeO_2 at ambient conditions are reached. In coesite, the largest change in an individual O–Si–O angle is smaller than in quartz, whereas the tetrahedral edges change more than in quartz (because of the larger changes in the Si–O bond lengths).

When the distortion of the tetrahedra is measured by quadratic elongation (Robinson, Gibbs and Ribbe, 1971), the percent increase becomes progressively larger with higher pressures (Levien, Prewitt and Weidner, 1980). Compression of the quartz structure is thus accomplished mainly at first by tetrahedral tilting (see section Inter-tetrahedral features: General), attended increasingly by tetrahedral distortion, as stated by Levien, Prewitt,

Table 6. Tetrahedral distortion indices.

Pressure/GPa	DI(TO)[a]	DI(OTO)[a]	DI(OO)[a]
a) SiO_2, quartz			
Levien, Prewitt and Weidner (1980):			
10^{-4}	0.003	0.006	0.005
2.07	0.002	0.008	0.006
3.76	0.003	0.011	0.009
4.84	0.003	0.014	0.009
5.58	0.003	0.015	0.010
6.16	0.001	0.017	0.011
This study:			
10^{-4}	0.003	0.005	0.004
4.0	0.003	0.012	0.008
7.2	0.005	0.018	0.013
10.2	0.005	0.026	0.017
	$\langle 0.003(1) \rangle$[b]		
b) GeO_2, quartz-type			
Smith and Isaacs (1964):			
10^{-4}	0.001	0.025	0.017
This study:			
10^{-4}	0.000	0.025	0.017
1.07	0.001	0.028	0.019
2.18	0.002	0.032	0.022
3.74	0.001	0.035	0.024
4.53	0.001	0.037	0.025
5.12	0.002	0.039	0.026
5.57	0.006	0.042	0.026
	$\langle 0.002(2) \rangle$[b]		

[a] $\left(\sum_{i=1}^{m} |x_i - \langle x \rangle|\right) \Big/ m\langle x \rangle$, with x_i individual and $\langle x \rangle$ mean tetrahedral bond length TO, tetrahedral edge length OO, and tetrahedral angle OTO, respectively (Baur, 1974).

[b] Mean value, e.s.d. in parenthesis.

and Weidner (1980). In the following the distortions are evaluated with the help of Baur's (1974) distortion indices DI(TO), DI(OTO) and DI(OO) (Table 6). They describe the distortions in bond lengths, bond angles and tetrahedral edges, respectively, as mean deviations from their average values. No significant changes appear in DI(TO), this parameter is even similarly small in both quartz-type structures. However, DI(OTO) and DI(OO) show pronounced variations (Table 6, Fig. 11). At ambient conditions they are distinctly smaller and more nearly equal in SiO_2 than GeO_2. Again, for SiO_2 at 10 GPa they reach the values of GeO_2 at normal

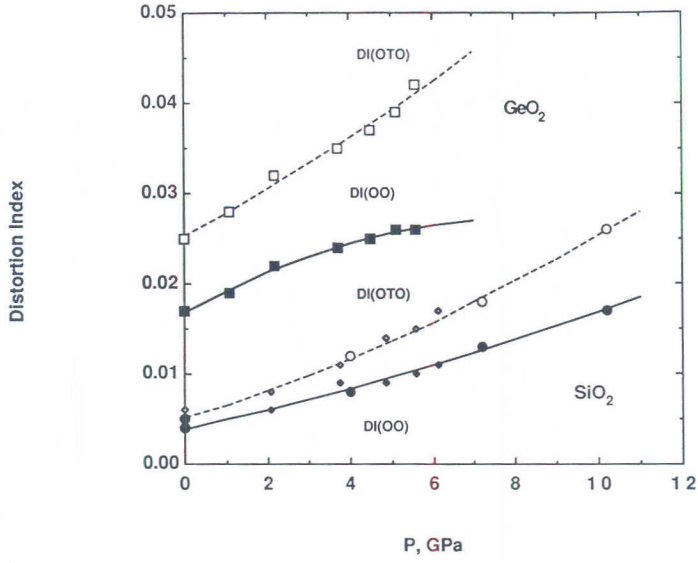

Fig. 11. The intra-tetrahedron distortion, indicated by the distortion indices of Baur (1974) (for definitions compare footnote [a] in Table 6). SiO_2: ○, ● this study; ◇, ◆ Levien, Prewitt and Weidner (1980); GeO_2: this study. At 10 GPa the magnitudes of the distortions for the SiO_4 tetrahedron equals that of the GeO_4 one at ambient pressure.

pressures. The latter data follow the trend in quartz, with further rise of DI(OTO) and a flattening of DI(OO) (Fig. 11). In coesite under pressure there is no or only little increase of the respective quantities.

The distortions of the tetrahedra proceed with a decrease in their volumes. A rough estimate of their mean volume compressibilities for all three compounds by means of

$$\bar{\beta}_{P_0,P} = \frac{-2}{V_0 + V_p} \cdot \frac{V_p - V_0}{P - P_0} \tag{6}$$

yields

$1.0 \cdot 10^{-3}$ GPa^{-1} for quartz ($P = 10.2$ GPa), (7)

$2.6 \cdot 10^{-3}$ GPa^{-1} for quartz-type GeO_2 ($P = 5.6$ GPa), and (8)

$2.6 \cdot 10^{-3}$ GPa^{-1} for coesite ($P = 5.2$ GPa). (9)

These values demonstrate the expected rigidity of the SiO_4 and GeO_4 tetrahedra compared with other cation polyhedra (Hazen and Finger, 1982,

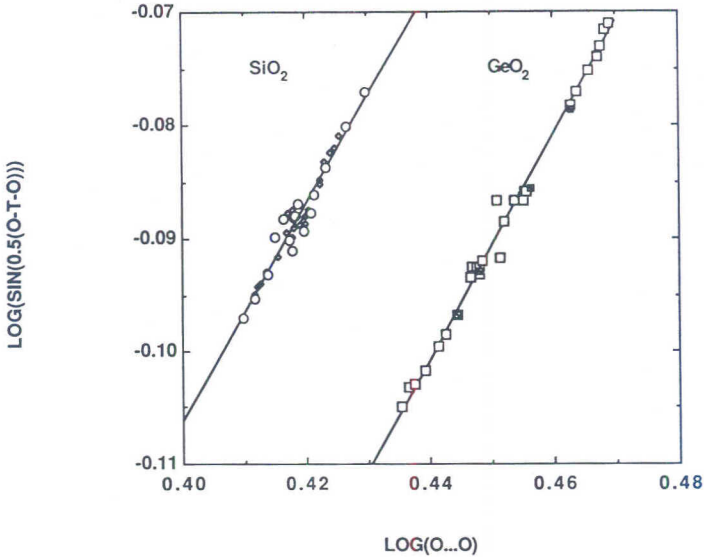

Fig. 12. Correlation of intra-tetrahedron O–T–O angles and O...O distances. The correlations found for ambient-pressure silicates and germanates by Louisnathan and Gibbs (1972) and Hill, Louisnathan and Gibbs (1977), apply as well to high-pressure structural data. ○, □ This study; ◇ Levien, Prewitt and Weidner (1980); ⊠ Smith and Isaacs (1964).

Table 7–2, pp. 152–154). Even though the actual values are not very precise, they indicate different compressibilities for the SiO_4 tetrahedra in the two SiO_2 polymorphs, which may be attributed to their different linkage topology. Whereas for coesite the Si–O bond lengths shrink, quartz experiences greater T–O–T and O–T–O bending, so the energy applied to bond bending cannot be applied to bond compression as well (Hazen and Finger, 1982, pp. 155/156; Liebau, 1983).

Despite all discussed deformations, no increase in the coordination number of the Si and Ge atoms even at the highest pressures applied takes place. However, an increase is observed by Liebau (1984) for other compounds.

Intra-tetrahedral features: Correlations

Only one of the correlations discussed in the literature (see beginning of Inter-tetrahedral features: Correlations) between quantities within the

tetrahedra was found to hold, moreover only for the quartz phases but not for coesite:

$$\log\left\{\sin\frac{1}{2}(\mathrm{O-T-O})\right\} = a + b\cdot\log\{d(\mathrm{O\ldots O})_\mathrm{T}\} \tag{10}$$

with $b = 1$, $a = \log\{2\langle d(\mathrm{T-O})\rangle\}$, $d(\mathrm{O\ldots O})_\mathrm{T}$ is a tetrahedral edge and $\langle d(\mathrm{T-O})\rangle$ is the mean value of the two T–O distances forming an O–T–O angle (Louisnathan and Gibbs, 1972; Hill, Louisnathan and Gibbs, 1977). For the pressure studies this becomes (Fig. 12)

$$\log\left\{\sin\frac{1}{2}(\mathrm{O-Si-O})\right\} = -0.490 + 0.958\cdot\log\{d(\mathrm{O\ldots O})_\mathrm{T}\} \tag{11}$$

($N = 40$, $r = 0.969$) for quartz and

$$\log\left\{\sin\frac{1}{2}(\mathrm{O-Ge-O})\right\} = -0.537 + 0.992\cdot\log\{d(\mathrm{O\ldots O})_\mathrm{T}\} \tag{12}$$

($N = 32$, $r = 0.996$) for GeO_2.

Both regressions clearly indicate that in the quartz-type structures under pressure the O–T–O angle variations are essentially only dependent upon the $d(\mathrm{O\ldots O})_\mathrm{T}$ distances, and thus are independent of the T–O bond lengths. Therefore the variations in the valence angles may be described by hard-sphere oxygen atoms moving upon the surface of hard-sphere T atoms. This is, however, not valid for coesite, demonstrating again the influence of the topology of the tetrahedral framework. It is noteworthy that both regressions are essentially the same as for the bulk of the silicates and germanates so far investigated at ambient conditions (Louisnathan and Gibbs, 1972; Hill, Louisnathan and Gibbs, 1977).

Brief comparison of structural variations under pressure and temperature

Elucidation of the thermal expansion of the low-quartz structure in crystal-chemical terms is complicated for several reasons:

(i) Structural changes with temperature in the whole stability region (under ambient pressure) of low quartz are small compared with those exhibited in the investigated pressure range. From 13 K to 843 K (just below the phase transition to high quartz at 846 K) the change in unit-cell volume is only 5%, compared with 18% at pressures up to 12.5 GPa (Fig. 4).

(ii) Atomic distances and bond lengths should be corrected for thermal motion at higher temperatures. However, atomic displacement parameters

for quartz are poorly determined up to now, as a comparison of these values from several authors even at room temperature reveals (Kihara, 1990). Therefore, together with the expected small changes, a discussion of variations in bond lengths, tetrahedral angles and tetrahedral distortion parameters is not warranted.

(iii) There is no data for GeO_2 with which to compare.

Low-temperature structural studies on quartz down to 13 K have been performed with higher precision than the present pressure experiments (Young and Post, 1962; Le Page, Calvert and Gabe, 1980; Lager, Jorgensen and Rotella, 1982). No significant changes in bond lengths and tetrahedral angles were found. The results of the high-temperature studies of Young (1962) and Kihara (1990) will not be interpreted in detail for the reasons given above under (ii). [But cf. Liebau (1983) for an attempt.] In the combined high-pressure, high-temperature study of Ogata, Takéuchi and Kudoh (1987) up to 2.3 GPa and 538 K no influence of temperature on structural changes could be deduced.

However, the different behaviour under pressure and temperature of the c/a ratio with cell volume (Fig. 4) already demonstrates differences in the distortion mechanisms of the tetrahedra under both influences. Additional indications for this can be drawn from the different slopes under pressure or temperature of the unit-cell volumes with Si–O–Si angle (Fig. 7) and of this angle with Si...Si distance (Fig. 9).[3] Thus, details in the structural changes taking place with thermal expansion and baric compression are not simply inverse.

Acknowledgement. One of the authors (J. G.) is greatly indebted to the Max-Planck-Gesellschaft for the grant of a fellowship. The high-pressure experiments on SiO_2 were performed at the Max-Planck-Institut für Festkörperforschung at Stuttgart. The experimental assistance by W. Dieterich and W. Böhringer (MPI Stuttgart) and the careful preparation of some drawings by R. A. Becker (Institut für Kristallographie, Aachen) is highly appreciated.

References

Akaogi, M., Navrotsky, A.: The quartz-coesite-stishovite transformations: New calorimetric measurements and calculation of phase diagrams. Phys. Earth Planet. Inter. **36** (1984) 124–134.

Bass, J. D., Liebermann, R. C., Weidner, D. J., Finch, S. J.: Elastic properties from acoustic and volume compression experiments. Phys. Earth Planet. Inter. **25** (1981) 140–158.

[3] One could argue that, with the exception of the c/a ratio and the volume of the unit cell, the quoted temperature data are falsified due to the missing corrections for thermal motion of the atoms. Such a correction, however, would have only minor influence on the slopes of the lines for the temperature data in Figs. 7 and 9. These data behave very similar, in spite of their great differences in precision and notwithstanding their different experimental sources, e.g. powder or single crystals, X-rays or neutrons, high- and low-temperature experiment.

Baur, W. H.: Bond length variation and distorted coordination polyhedra in inorganic crystals. Trans. Am. Cryst. Assoc. **6** (1970) 129–155.

Baur, W. H.: The geometry of polyhedral distortions. Predictive relationships for the phosphate group. Acta Crystallogr. **B30** (1974) 1195–1215.

Baur, W. H., Ohta, T.: The Si_5O_{16} pentamer in zunyite refined and empirical relations for individual silicon-oxygen bonds. Acta Crystallogr. **B33** (1982) 390–401.

Busing, W. R., Martin, K. O., Levy, H. A.: ORFEE, a FORTRAN crystallographic function and error program. ORNL-TM-306 (1964) Oak Ridge National Laboratory, Oak Ridge, Tennessee, USA.

Cromer, D. T., Mann, J. B.: X-ray scattering factors computed from numerical Hartree-Fock wave functions. Acta Crystallogr. **A24** (1968) 321–324.

D'Amour, H., Denner, W., Schulz, H.: Structure determination of α-quartz up to 68 $\times 10^8$ Pa. Acta Crystallogr. **B35** (1979) 550–555.

Donnay, J. D. H., Page, Y. Le: The vicissitudes of the low-quartz crystal setting or the pitfalls of enantiomorphism. Acta Crystallogr. **A34** (1978) 584–594.

Finger, L. W., King, H.: A revised method of operation of the single-crystal diamond cell and refinement of the structure of NaCl at 32 kbar. Am. Mineral. **63** (1978) 337–342.

Geisinger, K. L., Gibbs, G. V., Navrotsky, A.: A molecular orbital study of bond length and angle variation in framework structures. Phys. Chem. Minerals **11** (1985) 266–283.

Glinnemann, J.: Druckverhalten der Quarzstrukturen von SiO_2 und GeO_2 und eine neue Diamantstempelzelle. Thesis, Rheinisch-Westfälische Technische Hochschule Aachen, 1987.

Goodrum, J. W.: Solution top-seeding: Growth of GeO_2 polymorphs. J. Crystal Growth **13/14** (1972) 604–607.

Grimm, H., Dorner, B.: On the mechanism of the α-β-phase transformation of quartz. J. Phys. Chem. Solids **36**(5) (1975) 407–413.

Hamilton, W. C.: Angle settings for four-circle diffractometers. In: *International Tables for X-ray Crystallography, Vol. IV*. Eds. J. A. Ibers, W. C. Hamilton; pp. 336 + xi. Birmingham, Kynoch Press 1974.

Hazen, R. M., Finger, L. W.: *Comparative Crystal Chemistry – Temperature, Pressure, Composition and the Variation of Crystal Structure;* pp. 231 + xv. Chichester, John Wiley & Sons 1982.

Hazen, R. M., Finger, L. W., Hemley, R. J., Mao, H. K.: High-pressure crystal chemistry and amorphization of α-quartz. Solid State Commun. **72**(5) (1989) 507–511.

Hemley, R. J., Jephcoat, A. P., Mao, H. K., Ming, L. C., Manghnani, M. H.: Pressure-induced amorphization of crystalline silica. Nature **334** (1988) 52–54.

Hill, R. J., Gibbs, G. V.: Variation in d(T–O), d(T...T) and <TOT in silica and silicate minerals, phosphates and aluminates. Acta Crystallogr. **B35** (1979) 25–30.

Hill, R. J., Louisnathan, S. J., Gibbs, G. V.: Tetrahedral bond length and angle variations in germanates. Aust. J. Chem. **30** (1977) 1673–1684.

International Tables for Crystallography: Vol. A, Space-group symmetry. Ed. Th. Hahn; 2nd ed., pp. 878 + xvi. Dordrecht, D. Reidel 1989.

Jay, A. H.: The thermal expansion of quartz by X-ray measurements. Proc. Roy. Soc. A, **142** (1933) 237–247.

Jorgensen, J. D.: Compression mechanism in α-quartz structures – SiO_2 and GeO_2. J. Appl. Phys. **49**(11) (1978) 5473–5478.

Keller, R., Holzapfel, W. B.: Diamond anvil device for X-ray diffraction on single crystals under pressure up to 100 kilobar. Rev. Sci. Instrum. **48**(5) (1977) 517–523.

Kihara, K.: An X-ray study of the temperature dependence of the quartz structure. Eur. J. Mineral. **2** (1990) 63–77.

King, H. E., Jr., Finger, L. W.: Diffracted beam crystal centering and its application to high-pressure crystallography. J. Appl. Crystallogr. **12** (1979) 374–378.

King, H. E., Jr., LaPlaca, S. J., Dacol, F.: High pressure phase transition in GeO_2 alpha quartz: X-ray and Raman scattering evidence. In preparation. (1990).

King, H. E., Jr., Prewitt, C. T.: Improved pressure calibration system using the ruby R_1 fluorescence. – Rev. Sci. Instrum. **51**(8) (1980) 1037–1039.

Koepke, J.: Einkristall-Strukturuntersuchungen unter hydrostatischem Druck am Mineral Cordierit mit einer verbesserten Hochdruckzelle. Thesis, Universität Hamburg, 1985.

Koepke, J., Dieterich, W., Glinnemann, J., Schulz, H.: Improved diamond anvil high-pressure cell for single crystal work. Rev. Sci. Instrum. **56**(11) (1985) 2119–2122.

Koepke, J., Schulz, H.: Single crystal structure investigations under high-pressure of the mineral cordierite with an improved high-pressure cell. Phys. Chem. Minerals **13** (1986) 165–173.

Lager, G. A., Jorgensen, J. D., Rotella, F. J.: Crystal structure and thermal expansion of α-quartz at low temperatures. J. Appl. Phys. **53**(10) (1982) 6751–6756.

Lehmann, M. S., Larsen, F. K.: A method for location of the peaks in step-scan-measured Bragg reflexions. Acta Crystallogr. **A 30** (1974) 580–584.

Levien, L., Prewitt, Ch.: High-pressure crystal structure and compressibility of coesite. Am. Mineral. **66** (1981) 324–333.

Levien, L., Prewitt, Ch. T., Weidner, D. J.: Structure and elastic properties of quartz at pressure. Am. Mineral. **65** (1980) 920–930.

Liebau, F.: Einteilung und Mechanismen von Phasenumwandlungen. Fortschr. Miner. **61**(1) (1983) 29–84.

Liebau, F.: Pentacoordinate silicon intermediate states during silicate condensation and decondensation. Crystallographic support. Inorg. Chim. Acta **89** (1984) 1–7.

Liebau, F.: *Structural Chemistry of Silicates. Structure, Bonding, and Classification;* pp. 347 + xii. Berlin, Springer 1985.

Louisnathan, S. J., Gibbs, G. V.: Bond length variation in TO_4^{n-} tetrahedral oxyanions of the third row elements: T = Al, Si, P, S and Cl. Mat. Res. Bull. **7** (1972) 1281–1291.

Loveday, J. S., McMahon, M. I., Nelmes, R. J.: The effect of diffraction by the diamonds of a diamond-anvil cell on single-crystal sample intensities. J. Appl. Crystallogr. **23**(5) (1990) 392–396.

Megaw, H. D.: *Crystal Structures: A Working Approach*; pp. 563 + xviii. Philadelphia, Saunders 1973.

Merrill, L., Bassett, W. A.: Miniature diamond anvil pressure cell for single crystal X-ray diffraction studies. Rev. Sci. Instrum. **45**(2) (1974) 290–294.

Ogata, K., Takéuchi, Y., Kudoh, Y.: Structure of α-quartz as a function of temperature and pressure. Z. Kristallogr. **179** (1987) 403–417.

O'Keeffe, M., Hyde, B. G.: On Si–O–Si configurations in silicates. Acta Crystallogr. **B 34** (1978) 27–32.

O'Keeffe, M., Hyde, B. G.: The role of nonbonded forces in crystals. In: *Structure and Bonding in Crystals, Vol. I.* Eds. M. O'Keeffe, A. Navrotsky; pp. 327 + xviii. New York, Academic Press 1981.

Page, Y. Le, Calvert, L. D., Gabe, E. J.: Parameter variation in low-quartz between 94 and 298 K. J. Phys. Chem. Solids **41** (1980) 721–725.

Page, Y. Le, Donnay, G.: Refinement of the crystal structure of low-quartz. Acta Crystallogr. **B 32** (1976) 2456–2459.

Piermarini, G. J., Block, S., Barnett, J. D.: Hydrostatic limits in liquids and solids to 100 kbar. J. Appl. Phys. **44**(12) (1973) 5377–5382.

Robinson, K., Gibbs, G. V., Ribbe, P. H.: Quadratic elongation: A quantitative measure of distortion in coordination polyhedra. Science **172** (1971) 567–570.

Ross, N. L., Meagher, E. P.: A molecular orbital study of $H_6Si_2O_7$ under simulated compression. Am. Mineral. **69** (1984) 1145–1149.

Schomaker, V., Marsh, R.: On evaluation the standard deviation of U_{eq}. Acta Crystallogr. **A 39** (1983) 819–820.

Smith, G. S.: On the regularity of the tetrahedra in quartz. Acta Crystallogr. **16** (1963) 542–545.

Smith, G. S., Alexander, L. E.: Refinement of the atomic parameters of α-quartz. Acta Crystallogr. **16** (1963) 462–471.

Smith, G. S., Isaacs, P. B.: The crystal structure of quartz-like GeO_2. Acta Crystallogr. **17** (1964) 842–846.

Sowa, H.: The oxygen packings of low-quartz and ReO_3 under high pressure. Z. Kristallogr. **184** (1988) 257–268.

Stewart, J. M., Kruger, G. J., Ammon, H. L., Dickinson, C., Hall, S. R.: The X-ray system – version of June 1972, updated June 1974. Technical report TR – 192 of the computer science center, University of Maryland 1972.

Tattevin, H., Syono, Y., Kikuchi, M., Kusaba, K., Velde, B.: Shock deformation of alpha quartz: laboratory experiments and TEM investigation. Eur. J. Mineral. **2** (1990) 227–234.

Will, G., Parrish, W., Huang, T. C.: Crystal-structure refinement by profile fitting and least-squares analysis of power diffractometer data. J. Appl. Crystallogr. **16** (1983) 611–622.

Wright, A. F., Lehmann, M. S.: The structure of quartz at 25 and 590° C determined by neutron diffraction. J. Solid State Chem. **36** (1981) 371–380.

Young, R. A.: Final report, mechanism of the phase transition in quartz. Solid State Sciences Division Air Force Office of Scientific Research, Washington, D. C., 1962.

Young, R. A., Post, B.: Electron density and thermal effects in alpha quartz. Acta Crystallogr. **15** (1962) 337–346.

Zachariasen, W. H., Plettinger, H. A.: Extinction in quartz. Acta Crystallogr. **18** (1965) 710–714.

Zemann, J.: The shortest known interpolyhedral O–O distance in a silicate. Z. Kristallogr. **175** (1986) 299–303.

Zucker, U. H., Perenthaler, E., Kuhs, W. F., Bachmann, R., Schulz, H.: PROMETHEUS. A program system for investigation of anharmonic thermal vibrations in crystals. J. Appl. Crystallogr. **16** (1983) 358.